

STUDY OF THE EFFECT OF IMPURITIES AND HEAT TREATMENTS ON THE STRUCTURE OF Se-As-EuF₃, Se-Te-Sm AND Ge₂Sb₂Te₅ FILMS BY X-RAY DIFFRACTION AND RAMAN SPECTROSCOPY

S.N. GARIBOVA^{1,2}, A.I. ISAYEV¹, S.I. MEKHTIYEVA¹,
S.U. ATAYEVA¹, S.S. BABAYEV¹

¹*G.M. Abdullayev Institute of Physics of Azerbaijan NAS 131, H. Javid ave., Baku, AZ 1143*

²*Department of Physics and Electronics, Khazar University 41, Mehseti str., AZ1096,
Baku Azerbaijan*

sqaribova1@gmail.com

The local structure of film samples of the Se₉₅As₅, Se₉₅Te₅ and Ge₂₀Sb_{20.5}Te₅₁ chalcogenide semiconductors have been studied by X-ray diffraction and Raman spectroscopy. The effect of EuF₃ and Sm impurities on the structure of Se₉₅As₅, Se₉₅Te₅ and the effect of heat treatment at various temperatures on structure of Ge₂₀Sb_{20.5}Te₅₁ thin films have been studied. It was shown that Ge₂₀Sb_{20.5}Te₅₁ films obtained by thermal evaporation of an unheated glass substrate are amorphous, and those that underwent heat treatment at 220 and 400 °C transforms into a crystalline phase with a cubic and hexagonal structure. The chemical bonds and the basic structural elements that form the matrix of the studied materials, as well as the changes that occur in them upon the heat treatment and addition of impurities have been determined.

Keywords: glassy semiconductors, local structure, charged defects, memory effect.

PACS: 78.66.Jg, 72.15.Rn, 61.05.C, 73.20.Hb

1. INTRODUCTION

Interest in chalcogenide glassy semiconductors (CGS) appeared after semiconductor properties were first discovered in these materials, which combined with the properties of the glassy state [1]. CGS promising materials have the ability to change their electrical, photoelectric and optical properties under the influence of light, i.e. change the refractive index of light, the edge of optical absorption. Thanks to which they are widely used as active materials in various electrical switches, storage devices, in infrared (IR) technology and acousto-optical devices.

Switching and memory effects in chalcogenide glassy semiconductors have long been known, but the physics of these effects is still unknown. Recently, interest has increased in the development of non-volatile memory elements based on the chalcogenide glass-crystal phase transition, which allows a reversible phase change between a stable amorphous and crystalline state.

The memory elements based on CGS are called variable phase state or phase memory - Phase Change Memory (PCM), Phase Change Random Access Memory (PRAM) and Ovonyx Unified Memory (OUM). The short recording time and large optical contrast between the amorphous and crystalline states made it possible to use Ge₂Sb₂Te₅ materials to create rewritable CDs, DVDs, and Blu-ray discs, which demonstrated the stability and high speed of phase transitions in the materials of this system [2-4].

This work is devoted to the study of the local structure at the level short-range and medium-range order of binary and triple chalcogenide materials. The CGS systems Se-As and Se-Te doped with EuF₃ and Sm impurities, as well as Ge₂₀Sb_{20.5}Te₅₁ have been chosen as the study objects.

The choice of rare-earth elements as an impurity is due to the fact that, as chemically active elements, they can form new structural elements with selenium atoms, i.e. can lead to a change in the local structure at the level of short-range and medium-range order and thus affect the physical properties. The Ge-Sb-Te triple chalcogenide material, depending on the temperature and the technological regime of sample preparation, can be in amorphous and two crystalline phases - cubic and hexagonal, which should be accompanied by changes in the parameters of short-range and medium-range order. X-ray diffraction and Raman spectroscopy have chosen as the research methods. Such studies make it possible to determine short-range and medium-range order parameters, as well as chemical bonds and structural elements of the matrix of samples in both amorphous and crystalline states and changes depending on the chemical composition and the presence of impurities.

2. EXPERIMENTS AND SAMPLE PREPARATION

Chalcogenide materials Se-As-EuF₃, Se-Te-Sm and Ge-Sb-Te were obtained by fusion of elementary substances of high purity in vacuumized up to 10⁻⁴ Torr quartz ampoules. The synthesis was carried out at a temperature of 900 °C for 10 hours with holding for at least 5 hours in a rotary kiln, followed by cooling in the off-furnace mode. The samples for measurements were films 0.5, 0.75 and 1.5 μm thicknesses and 3–8 μm thickness, obtained by thermal evaporation at a rate of 0.2–0.5 μm/s in vacuum on a glass substrate at a pressure of 10⁻⁴ Torr, as well as bulk samples 1.5 mm thick. X-ray diffraction analysis was performed using a “Bruker” D2Phaser diffractometer and CuKα-rays with a radiation wavelength of λ = 1.5406 · 10⁻¹⁰ m in the angle range 2θ = 5–80°.

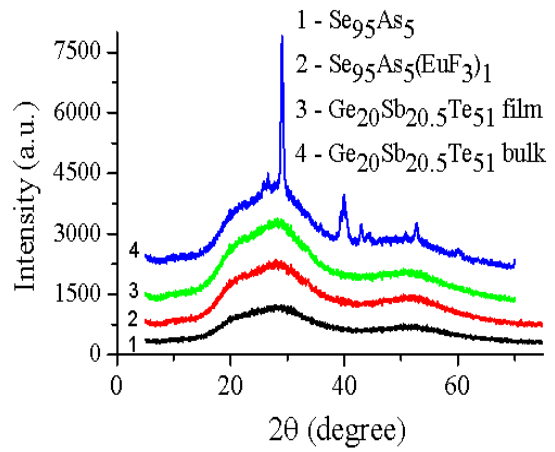
Structural studies and calculations were carried out using the EVA and TOPAZ programs. Raman spectra were studied on a three-dimensional confocal Raman microscope Nanofinder 30 (Tokyo Instr.), the excitation wavelength was 532 nm. The radius of the cross section of the laser beam incident on the film was ~ 4 μm. The radiation receiver was a cooled CCD camera (-70°C) operating in the photon counting mode with exposure time 10–20 s at a laser radiation power of 4 mW, and the spectral resolution error 0.5 cm⁻¹. The experiments were carried out at room temperature, and after heat treatment of the samples at 120, 220, 400 °C for 30 min.

3. EXPERIMENTAL RESULTS AND DISCUSSION

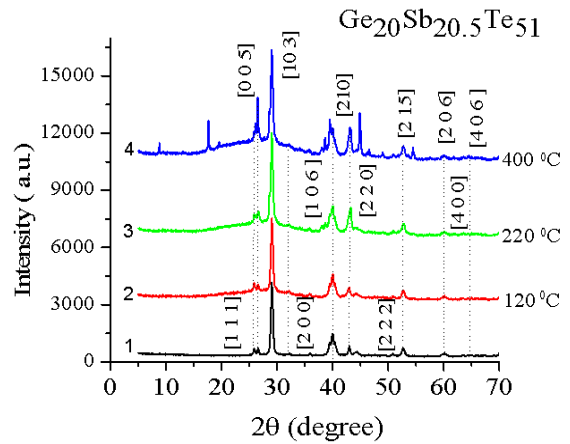
3.1. X-Rays diffraction analysis of the structure Se₉₅As₅<EuF₃> and Ge₂₀Sb_{20.5}Te₅₁ films.

Fig. 1 shows the angular distributions of the X-ray diffraction intensity of the samples Se₉₅As₅<EuF₃> and Ge₂₀Sb_{20.5}Te₅₁ systems. X-ray diffraction patterns (XRD) of the Se₉₅As₅ and Se₉₅As₅(EuF₃)₁ 8 μm, Ge₂₀Sb_{20.5}Te₅₁ 0.5 μm and 1.5 mm thickness samples are presented in Fig.1a. While Fig.1b are XRD patterns of the Ge₂₀Sb_{20.5}Te₅₁ 0.5 - 0.75 μm and 1.5 mm thickness.

As can be seen from the XRD patterns, film samples at room temperature (Fig. 1a, curves 1, 2 and 3) have a broad maximum at 2θ (θ is the Bragg angle) located in the range 15–38 °, which indicates their amorphous. Most CGSs have a similar extent, including Se-Te and Se-Te-Sm. From the XRD patterns of Se-As-EuF₃ and Se-Te-Sm have been determined the “quasiperiod” (R) of the structure of fluctuations in the atomic density [5–7], the repetition of which in a certain region can cause the appearance of the first sharp diffraction peak (FSDP), the length of the correlation (L), in which the frequency fluctuation of the density is preserved, and the diameter of the nanovoids (D) or a region with a reduced atomic density.



a)



b)

Fig.1. XRD patterns of (a) Se₉₅As₅, Se₉₅As₅(EuF₃)₁ and Ge₂₀Sb_{20.5}Te₅₁ chalcogenide samples at room temperature, (b) Ge₂₀Sb_{20.5}Te₅₁ before (curve 1) and after the treatment temperature (curves 2, 3, 4).

The values of the parameters characterizing the structure of the studied films are given in the table 1.

Table 1.

The values of short-range and medium-range orders parameters of Se-As-EuF₃ and Se-Te-Sm film samples.

	R, Å	L, Å	D, Å
Se ₉₅ As ₅	3.177	6.5443	3.654
Se ₉₅ As ₅ +1at%EuF ₃	3.318	6.0349	3.816
Se ₉₅ Te ₅	4.02	12.94	4.63
Se ₉₅ Te ₅ +1at%Sm	3.35	8.16	3.85

The XRD pattern of the Ge-Sb-Te bulk sample 1.5 mm thick (Fig. 1a, curve 4) shows that, before the treatment temperature, the presence of peaks at angles of 25.7 °, 29.7 °, 42.8 ° and 52.9 ° indicates cubic phase of the crystal structure. Figure 1b shows the XRD pattern of the Ge₂₀Sb_{20.5}Te₅₁ samples before (curve 1) and after the treatment temperature (curves 2, 3, 4). XRD pattern of a bulk sample to the

processing temperature (Fig. 1b, curve 1) obtained in the off-furnace mode has certain maxima (reflections) at angles of 25.7° (111), 29.7° (200), 42.8° (220) and 52.9° (222), which corresponds to reflections of the first and second order in the metastable face-centered cubic (FCC) phase along the (111) direction [8, 9]. At a temperature of 120°C, the peaks in the film sample (curve 2 of Fig. 1b) remain almost unchanged, but

peaks appearing in the films (curves 3, 4 of Fig. 1b) indicate crystallization. At a temperature of 220°C, the intensities of these peaks increase and new ones appear at 29.7° (103), 40.1° (106), 42.8° (210), 60.1° (206), 63.6° (400), the intensities of which also increase with a further increase in processing temperature (up to 400 °C). The positions of the fixed peaks correspond to the results of [8–10] and indicate the origin of structural changes in the sample at the stable hexagonal phase (HEX - phase structure).

The materials of the Ge-Sb-Te system have a low glass-forming ability and are easy to crystallize, and to obtain such a material in an amorphous state, it is necessary to cool the melt in a few tens or hundreds of nanoseconds. It is the high crystallization rate that allows in modern memory cells to record information in less than 50 ns. However, with decreasing temperature, the crystallization time increases exponentially and is about 100 years at room temperature [11]. Therefore, the materials of the Ge-Sb-Te system are successfully used in modern storage media.

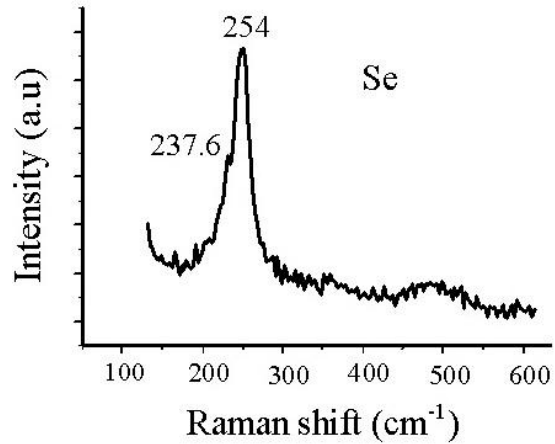
The analysis of Ge₂₀Sb_{20.5}Te₅₁ XRD patterns indicates that the film samples are amorphous to the processing temperature, while the bulk sample has a crystalline structure, in particular a cubic one. After the treatment temperature (at 120°C), the film structures crystallize, partially transforming into a cubic structure. With a further increase in temperature to 220 °C, peaks appear in the structure of the films, indicating a hexagonal phase. At 400 °C the Ge₂₀Sb_{20.5}Te₅₁ film sample transfers to the stable hexagonal phase.

3.2. Raman scattering of Se₉₅As₅<EuF₃>, Se₉₅Te₅<Sm> and Ge₂₀Sb_{20.5}Te₅₁ amorphous and crystalline films.

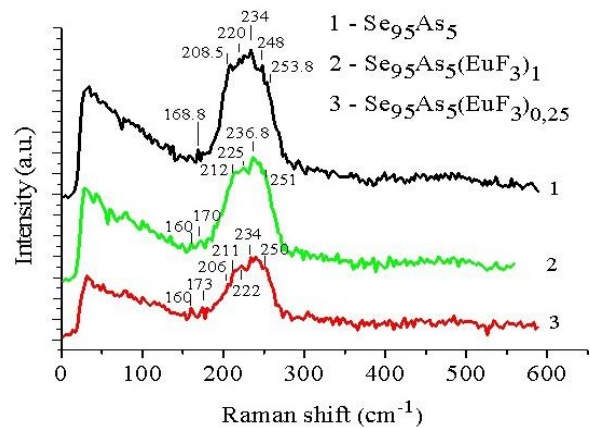
Fig. 2 shows the Raman scattering in films 3-8 μm thickness of amorphous selenium (Fig. 2a) and Se₉₅As₅(EuF₃)_x (x = 0; 0.5; 1 at%) (Fig. 2b). It can be seen that the spectrum of amorphous selenium consists of a broad maximum at a frequency of 254 cm⁻¹ and a narrow maximum at 237.6 cm⁻¹, which correspond to vibrations of ring Se₈ and chain -Se - Se- molecules [12, 13]. With the addition of arsenic to selenium, the maximum at 254 cm⁻¹ weakens and peaks appear in the frequency range 209–220 cm⁻¹, which is partially due to the destruction of ring molecules and the formation of an As₄Se₄ type molecular fragment. In addition, a peak appears at 225cm⁻¹ and is attributed to AsSe₃ structural elements [12, 14].

The weak maximum at 170 cm⁻¹ observed in all spectra shown in Fig. 2b, is attributed to vibrations of the As - As homeopolar bond [15]. The introduction of the EuF₃ impurity leads to the appearance of narrow peaks in the Raman spectrum of Se₉₅As₅ films, which is associated with the formation of new structural elements with the participation of europium atoms. Since europium atoms as a chemically active element form chemical bonds with selenium atoms. In this case, the peak at 254 cm⁻¹ is strongly attenuated,

which is due to the fact that the participation of europium atoms leads to a more efficient destruction of ring selenium molecules. In addition, it is assumed that europium atoms lead to the crosslinking of the ends of the polymer chains into a pyramidal structure and the peaks at frequencies of 220.7 cm⁻¹, 211 cm⁻¹ and 160.4 cm⁻¹ are associated with vibrations of the EuSe₃, EuSe_{3/2} pyramidal structural elements and Eu - Se bonds, respectively.



(a)



(b)

Fig.2. Raman spectra of (a) Se and (b) Se-As, Se-As-EuF₃ amorphous film samples.

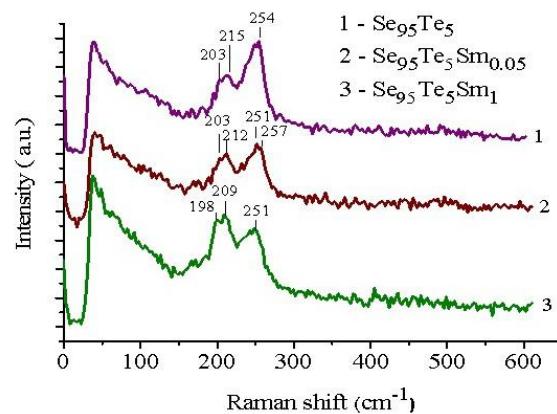
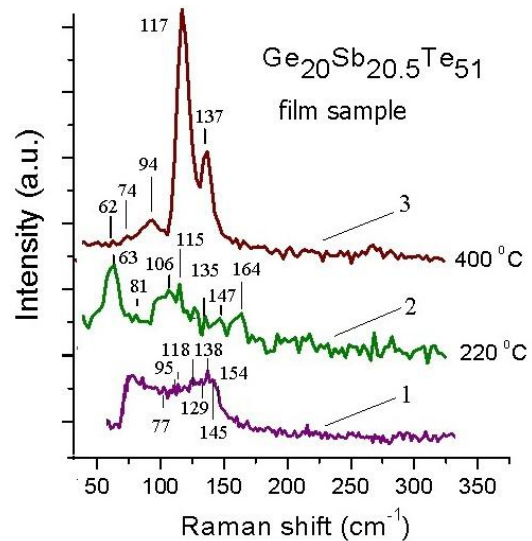


Fig.3. Raman spectra of Se-Te and Se-Te-Sm amorphous film samples.

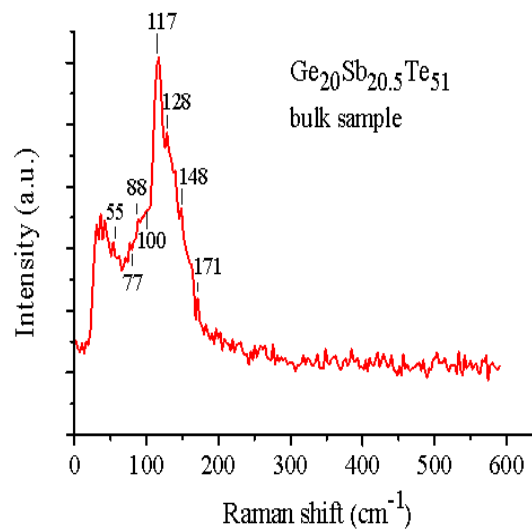
The Raman spectrum of amorphous $\text{Se}_{95}\text{Te}_5$ doped with samarium is shown in Fig. 3. Peaks at 211.7 and 253.3 cm^{-1} are observed in the $\text{Se}_{95}\text{Te}_5\text{CGS}$ composition. As already noted, the peak at 253.3 cm^{-1} belongs to ring selenium molecules, and the peak at 211.7 cm^{-1} , according to [16], corresponds to vibrations of the Se – Te bond. It is known that amorphous selenium consists of long polymer chains and eight-membered rings, inside of which covalent bonds exist between atoms, and between various structural elements the van-der-Waals bonds [17]. The addition of tellurium to amorphous selenium leads to partial destruction of ring molecules and shortening of polymer chains. As a result, the number of Se – Se bonds decreases, and Se – Te bonds are formed, accompanied by the appearance of a band of 211.7 cm^{-1} corresponding to the indicated bonds. As can be seen from the figure, doping with samarium changes the shape and intensity of the peaks in the Raman spectrum. In this case, a decrease in the intensity of the band peak at 254 cm^{-1} and an increase in the band peak at 211.7 cm^{-1} , as well as a slight expansion of the latter toward the low-frequency side of the spectrum, are observed. The latter, apparently, is associated with the chemical activity of samarium atoms, which form bonds with both selenium and tellurium (Sm – Se, Sm – Te, Se – Sm – Te), as well as pyramidal structural elements involving samarium atoms ($\text{SmSe}_x\text{Te}_{3-x}$). The frequencies of the vibrational modes corresponding to the indicated bands are close to each other and overlapping form bands.

Fig. 4a shows the Raman spectrum of a bulk 1.5 mm thick and Fig. 4b film $0.5\text{--}0.75\text{ }\mu\text{m}$ thickness samples of $\text{Ge}_{20}\text{Sb}_{20.5}\text{Te}_{51}$ obtained at room temperature (Fig. 4b curve 1) and subjected to heat treatment at $220\text{ }^\circ\text{C}$ (curve 2) and $400\text{ }^\circ\text{C}$ (curve 3). The spectrum of films at room temperature consists of a wide band covering the frequency range $75\text{--}175\text{ cm}^{-1}$ with weak maxima at $95, 105, 118, 129, 147,$ and 160 cm^{-1} (Fig. 4b, curve 2). The maxima at $160, 149, 129\text{ cm}^{-1}$, with some deviations, were observed in the Raman spectrum of bulk sample (Fig. 4a) and films obtained at room temperature and heat-treated at $220\text{ }^\circ\text{C}$ (Fig. 4b, curve 1, 2), and maximums at $115\text{--}117\text{ cm}^{-1}, 74\text{--}90\text{ cm}^{-1}$ in the spectrum of all samples. A number of works [18–25] are devoted to studying the features of the Raman scattering spectrum of amorphous and crystalline $\text{Ge}_2\text{Sb}_2\text{Te}_5$ samples. The authors of [18, 22] attributed the 160 cm^{-1} peak to vibrations of defective octahedral structural elements based on Ge. The authors of [22] calculated the Raman spectrum of amorphous and cubic crystals of the $\text{Ge}_2\text{Sb}_2\text{Te}_5$ structure using *ab initio* phonon methods and an empirical model of bond polarizability. They concluded that the observed features of both amorphous and crystalline $\text{Ge}_2\text{Sb}_2\text{Te}_5$ can be attributed to vibrations of defective octahedra. The signs of tetrahedra in the Raman scattering spectrum of amorphous samples are covered by a large cross section of the Raman scattering of defective octahedra. The authors of [19] attributed this peak to vibrations of the Sb – Sb homeopolar bond,

and the authors of [20] to the crystallization of the samples. The authors [22, 24–25] associated the maximum at 160 cm^{-1} with activation of the A_{1g} vibrational modes and their appearance was considered a sign of the formation of crystalline structural elements.



(a)



(b)

Fig.4. Raman spectra of (a) Ge-Sb-Te bulk sample before and (b) Ge-Sb-Te film samples after the processing temperature.

The band localized at $\sim 150\text{ cm}^{-1}$ (in our studies at $\sim 147\text{ cm}^{-1}$) is directly related to the Sb_2Te_3 and partially to the pyramidal SbTe_3 structural element [18]. The band with maxima of $\sim 145\text{--}150\text{ cm}^{-1}$ was attributed by other researchers to vibrations of the Sb – Te bond in the SbTe_3 pyramidal structural element [25] or in octahedrally coordinated Sb atoms [22]. A wide band at 150 cm^{-1} was also observed in [26] and associated with vibrations of the Te – Te homeopolar bond. The authors of this work noted that this band is observed only in samples subjected to low-

temperature annealing. A peak at 150 cm^{-1} of the corresponding Te – Te bond extension modes have not observed in the Raman spectrum of bulk Ge₂Sb₂Te₅ samples [20], which has considered a sign of good crystallization of bulk samples.

Peaks at frequencies of $\sim 127\text{--}129\text{ cm}^{-1}$ in the Raman spectrum have been observed in all Ge₂Sb₂Te₅ samples except for the film, which is subjected to heat treatment at $400\text{ }^\circ\text{C}$. The position of this peak is very close to the maximum at 125 cm^{-1} observed in [18], which the author of [27], taking into account the results of Raman scattering studies in a-GeTe thin films [28], attributed the A₁ mode of the GeTe_{4-n}Ge_n composition ($n = 1, 2$) - corner-sharing tetrahedra. The existence of tetrahedral units of GeTe_{4-n}Ge_n ($n = 1, 2$), including Ge-Ge homeopolar bonds, was also reported in [29] as the results of the EXAFS study. Tetrahedral structural elements are inherent in binary chalcogenides of the GeSe₂ and GeS₂ type [30, 31].

As can be seen from Fig. 4 peak at $115\text{--}118\text{ cm}^{-1}$ is very weakly observed in the Raman spectrum of films (Fig. 4b) obtained at room temperature (curve 1), become pronounced after heat treatment at $220\text{ }^\circ\text{C}$ (curve 2) and strongly amplifies after thermal processing at $400\text{ }^\circ\text{C}$ (curve 3). The indicated peak will also be observed rather intensively in bulk sample (Fig. 4a). The indicated peak was also observed at $\sim 115\text{ cm}^{-1}$ in [20], and the peak at 120 cm^{-1} in [21, 22, 24, 32] and was attributed to the vibration of defective octahedra.

Weak peaks in the frequency range $74\text{--}90\text{ cm}^{-1}$ observed in the Raman spectrum of all samples were also observed by the authors of [27, 34–35.] and the authors of [27], taking into account the results of studies presented in [33], were connected by the E mode of the GeTe₄ tetrahedron.

In the samples that underwent heat treatment at $220\text{ }^\circ\text{C}$, the peaks at $\sim 127\text{--}129\text{ cm}^{-1}$ and $\sim 145\text{--}150\text{ cm}^{-1}$ are attenuated and peaks appear at $\sim 105\text{--}106\text{ cm}^{-1}$ and $\sim 135\text{--}137\text{ cm}^{-1}$ of vibrational modes for crystalline phases cubic structure (FCC configuration - Fig. 1b). According to the authors of [9], the first peak can be attributed to vibrations of A₁ mode of corner-sharing GeTe₄ tetrahedra and the second to GeTe_{4-n}Ge_n ($n = 1, 2$) tetrahedra. In the samples that underwent heat treatment at $400\text{ }^\circ\text{C}$, these peaks disappear and low-frequency peaks remain and pronounced peaks appear at 117 and 137 cm^{-1} , i.e. crystalline phases with a hexagonal structure are formed (HEX configuration - Fig. 1b).

From the above interpretation of the results of studying the Raman spectrum of Ge₂₀Sb_{20.5}Te₅₁ samples obtained by various methods (by thermal

evaporation and cooling of the alloy), as well as crystallized by heat treatment, it follows that their positions of several peaks coincide. This coincidence of the peaks in the Raman spectrum for various samples indicates the coincidence of the short-range order in the arrangement of atoms in them.

4. CONCLUSION

Using X-ray diffraction and Raman spectroscopy, the short-range and medium-range order features in the atoms arrangement of the Se₉₅As₅<EuF₃>, Se₉₅Te₅ <Sm> and Ge₂₀Sb_{20.5}Te₅₁ chalcogenide materials have been studied. In particular, the correlation length in the atoms arrangement, the “quasiperiod” of fluctuations in the atoms density on the scale of the correlation length, chemical bonds and the main structural elements that form the matrix of the studied materials have been determined.

It was established that the technological mode of sample preparation (melt cooling, thermal evaporation in vacuum) and heat treatment significantly affect the structure of Ge₂₀Sb_{20.5}Te₅₁. Film samples of Ge₂₀Sb_{20.5}Te₅₁ obtained by thermal evaporation on an unheated glass substrate are amorphous, heat-treated at 220 and $400\text{ }^\circ\text{C}$ pass into the crystalline phase with a cubic (FCC) and hexagonal (HEX) structure, and samples obtained by cooling the melt are partially crystallized.

The chemical bonds and the main structural elements that form the matrix of the studied objects, also the changes that occur in them with the heat treatment and addition of impurities have been determined. It was shown that the main structural elements of bulk sample and films obtained by thermal evaporation on an unheated glass substrate and thermally processed at $220\text{ }^\circ\text{C}$ are the defective octahedra, GeTe_{4-n}Ge_n ($n = 1, 2$) corner-sharing tetrahedral, the Sb₂Te₃ structural and the SbTe₃ pyramidal structural element.

ACKNOWLEDGMENTS

The authors are grateful to S.S. Babayev, I.R. Amiraslanov and the late E.R. Aliyeva for the help provided during the experiments.

FINANCING

The work was carried out in the Innovation sector of the G.M. Abdullayev Institute of Physics of Azerbaijan NAS.

-
- [1] B.T. Kolomies, N.A. Qoryunova. 1955. Tech. Phy. Letter, 25 (6), 984 [in Russian].
- [2] M. Wuttig, N. Yamada. 2007. Nature Mater., 6, 824.
- [3] W. Welnic, M. Wuttig, 2008. Materials Today, 11 (6), 20.
- [4] D. Lencer, M. Salinga, M. Wuttig. 2011. Adv. Mater., 23, 2030.
- [5] T.S. Kavetskyy, O.I. Shpotyuk. 2007. J. Optoelectron. Adv. Mater., 7, 2267.
- [6] O.I. Shpotyuk, A. Kozdras, T.S. Kavetskyy, J. Filipecki, 2006. J. NonCryst. Sol., 352, 700.
- [7] S.R. Elliott. 1992. J. Phys. Cond. Matt., 38, 7661.

- [8] V. Bragaglia, B. Jenichen, A. Giussani, K. Perumal, H. Riechert, R. Calarco. 2014. Appl. Phys., 116, 054913.
- [9] X. Zemin, C. Chaonan, W. Zhewei, W. Ke, C. Haining, Y. Hui. 2018. RSC Advances., 8, 21040-21046.
- [10] Zhang Ting, Liu Bo, Xia Ji-Lin, Song Zhi-Tang, Feng Song-Lin, Chen Bomy. 2004. Chin. Phys. Lett., 21(4), 741-744.
- [11] A.L. Lacaíta. 2006. Sol. St. Electron., 50, 24.
- [12] V. Kovanda, M. Vicek, H. Jain. 2003. J. Non-Cryst. Sol., 88, 326.
- [13] V.I. Mikla. 1997. J. Phys. Condens. Matter, 9, 9209.
- [14] W. Bues, M. Somer, W. Brockner, Z. Naturforsch. 1980. 35B, 1063.
- [15] C. Zha, R. Wang, A. Smith, A. Prasad, R.A. Jarvis, Luther-Davies, B. (2007). J. Mater Sci.: Mater. Electron., 18, 389.
- [16] A. Mendoza-Galvan, E. Garcia-Garcia, Y.V. Vorobiev, Gonzalez-Hernandez. J. Microelectron. Engin. 2000. 51, 677.
- [17] Q.B. Abdullayev, J.S. Abdinov. 1975. Selenium Physics, Baku, Science [in Russian].
- [18] K. Shportko, L. Revutska, O. Paiuk, J. Baran, A. Stronski, A. Gubanova, E. Venger. (2015) Optical Mater. (Amst), 73, 489 - 496.
- [19] B. Liu, Z. Song, T. Zhang, S. Feng. Chen B. 2004. Chin. Phys., 13, 1947.
- [20] E. Cho, S. Yoon, H.R. Yoon, W. Jo. 2006. J. Korean Physical Society, 48 (6), 1616-1618.
- [21] V. Bragaglia, K. Holldack et al. 2016. Scientific Reports, 6: 28560.
- [22] G.G. Sosso, S. Caravati, R. Mazzarello, M. Bernasconi. 2011. Phys. Rev., B83, 134201.
- [23] S.A. Kozyukhin, V.H. Kudoyarova, H.P. Nguyen et al. 2011. Phys. Status Solidi C 8, 9, 2688–2691.
- [24] G. Bulai, O. Pompilian et al. 2019. Nanomaterials, 9, 676.
- [25] P. Nemeč, V. Nazabal, A. Moreac, J. Gutwirth, L. Benes, M. Frumar. 2012. Mater. Chem. Phys., 136, 935-941.
- [26] J. Tominaga, N. Atoda. 1999. Jpn. J. Appl. Phys., 38, L322.
- [27] S. Kozyukhin, M. Veres, H.P. Nguyen, A. Ingram, V. Kudoyarova. 2013. Physics Procedia, 44, 82 – 90.
- [28] K.S. Andrikopoulos, S.N. Yannopoulos, A.V. Kolobov, P. Fons. J. Tominaga. 2006. J. Phys. Condens. Matter, 18.
- [29] G. Lucovsky, D.A. Baker, M.A. Paesler. Phillips J. C. 2007. J. Non-Cryst. Solids, 353, 1713.
- [30] S. Sugai. 1987. Phys. Rev. B: Condens. Matter, 35, 1345.
- [31] J. Koblar, B. Arlin, and G. Shau. 1999. Phys. Rev. B: Condens. Matter, 60.
- [32] E. Yalon, S. Deshmukh et al. 2017. Scientific Reports, 7: 15360.
- [33] K.S. Andrikopoulos, S.N. Yannopoulos, A.V. Kolobov, P. Fons, J. Tominaga. 2006. J. Phys. Condens. Matter, 18.
- [34] P. Nemeč, A. Moreac, V. Nazabal, M. Pavlišta, J. Prikryl, M. Frumar. 2009. J. Appl. Phys., 106, 103509.
- [35] H.R. Yoon, W. Jo, E. Cho, S. Yoon, M. Kim. 2006. J. Non-Cryst. Solids, 352, 3757–3761.

Received: 04.06.2021